Recruitment and Derecruitment During Acute Respiratory Failure

An Experimental Study

PAOLO PELOSI, MARI GOLDNER, ANDREW McKIBBEN, ALEX ADAMS, GIUDITTA ECCHER, PIETRO CAIRONI, SABINA LOSAPPIO, LUCIANO GATTINONI, and JOHN J. MARINI

Istituto di Anestesia e Rianimazione, Università degli Studi di Milano, Ospedale Maggiore Policlinico–IRCCS, Milan, Italy; and Department of Pulmonary and Critical Care Medicine, University of Minnesota, Regions Hospital, St. Paul, Minnesota

We aimed to elucidate the relationships between pleural (Ppl), esophageal (Pes), and superimposed gravitational pressures in acute lung injury, and to understand the mechanisms of recruitment and derecruitment. In six dogs with oleic acid respiratory failure, we measured Pes and Ppl in the uppermost, middle, and most dependent lung regions. Each dog was studied at positive end-expiratory pressure (PEEP) of 5 and 15 cm H_2O and three levels of tidal volume (V_T; low, medium, and high). For each PEEP–V_T combination, we obtained a computed tomographic (CT) scan at end-inspiration and end-expiration. The variations of Ppl and Pes pressures were correlated ($r = 0.86 \pm 0.07$, $p < 0.0001$), as was the vertical gradient of transpulmonary (P_L) and superimposed pressure ($r = 0.92$, $p < 0.0001$). Recruitment proceeded continuously along the entire volume–pressure curve. Estimated threshold opening pressures were normally distributed (mode = 20 to 25 cm H_2O). The amount of end-expiratory collapse at the same PEEP and P_L was significantly lower when ventilation was performed at high V_T. End-inspiratory and end-expiratory collapse were highly correlated ($r = 0.86$, $p < 0.0001$), suggesting that as more tissue is recruited at end-inspiration, more remains recruited at end-expiration. When superimposed pressure exceeded applied airway pressure (Paw), collapse significantly increased.

Keywords: ALI/ARDS; oleic acid; mechanical ventilation; computed tomography; volume pressure curve

Recent delineation of the underlying pathology of acute lung injury (ALI) and the acute respiratory distress syndrome (ARDS) has furthered progress toward understanding the relationship between mechanical ventilation and its effects on the injured lung. This knowledge has given rise to more precise definitions and classifications, as well as to concepts of barotrauma, volutrauma, and biotrauma (1). Our more complete scientific background has led to a modified approach to the clinical practice of mechanical ventilation that aims to reduce iatrogenicity and improve survival. Through this continuing feedback between laboratory investigation and refinement of therapy, it has now been convincingly established that tidal volumes (V_T) that generate high alveolar pressures are more deleterious than lower V_T (2). Despite that significant advance, several questions with the potential to further improve clinical outcome remain to be investigated.

One putative mechanism of pulmonary damage induced by mechanical ventilation is recurrent tidal collapse and reopening of lung units during the respiratory cycle (3, 4). If this concept proves correct, the directive to "open the lung and keep the lung open" (5) may beneficially impact ventilatory practice. However, several questions still remain. Do all ALI/ARDS patients have similar potential for recruitment? Moreover, if they differ, are recruitment maneuvers equally effective or indicated in all patients? Are descriptors of pulmonary mechanics, such as the volume–pressure (VP) curve, useful tools for understanding the underlying pathology and for selecting reasonable settings for mechanical ventilation in clinical practice?

In a collaborative effort of two groups (one from the United States and one from Europe), we designed experimental and clinical studies in which a similar methodology was applied to further elucidate the mechanisms of recruitment and derecruitment. Although the pathology of our experimental model (oleic acid in dogs) clearly differed from that of the majority of our patients (ARDS from a primary pulmonary origin), the "rules" governing recruitment and derecruitment appeared to be impressively similar in both settings, suggesting a mechanism common to both. This first report of our work describes the mechanisms of recruitment and derecruitment in our animal model, in which respiratory failure was induced by oleic acid injection. The second report describes our experience in the clinical setting.

METHODS

All techniques and procedures were approved by the Animal Care and Use Committee of Regions Hospital; the care and handling of the animals were conducted in accordance with the guidelines of the National Institute of Health.

Animal Instrumentation

We studied six adult mixed-breed dogs (mean weight: 25.6 ± 1.3 kg) of either sex, during anesthesia (sodium pentobarbital, 3 to 5 mg/kg/h) and paralysis (pancuronium bromide, 0.1 mg/kg). Each animal was orally intubated and mechanically ventilated (Puritan Bennet model 7200, Carlsbad, CA). Airway pressure (Paw) was measured (Validyne MP-45 $\pm$ 100 cm H_2O; Northridge, CA) from a side tap connected to the endotracheal tube, and inspiratory and expiratory flows were detected by a Fleisch type pneumotachograph (3719; Hans Rudolph, Kansas City, MO) attached to the corresponding limbs of the ventilator circuit.

The esophageal pressure (Pes) was measured by a multiperforated balloon catheter (10 cm long, filled with 1 ml of air) attached to a pressure transducer (Validyne MP-45 $\pm$ 50 cm H_2O). Appropriate position for the esophageal catheter was verified by the airway occlusion technique during spontaneous breathing under light anesthesia before paralysis (6). Systemic arterial pressure and heart rate were monitored by a femoral catheter and an electrocardiographic monitor, respectively. Vascular pressures were referenced to midchest level and measured at end-expiration. Arterial blood samples were analyzed at 37° C (model 168 blood gas analyzer; Corning, Medfield, MA) and corrected for body temperature.

To directly measure the pleural pressure (Ppl), we unilaterally inserted three flexible flat pressure sensors or "wafers" ($75 \times 55 \times 1.5$ mm) in the uppermost, the middle, and the most dependent parts of the chest cavity, by means of a single incision (4 cm length) in the

(*Received in original form July 5, 2000 and in revised form January 25, 2001*)

Correspondence and requests for reprints should be addressed to Prof. Luciano Gattinoni, Istituto di Anestesia e Rianimazione, Università degli Studi di Milano, Ospedale Maggiore di Milano–IRCCS, Via Francesco Sforza 35, 20122 Milano, Italy. E-mail: gattinon@polic.cilea.it

Am J Respir Crit Care Med Vol 164. pp 122–130, 2001
Internet address: www.atsjournals.org

sixth intercostal space. The pressure-sensing portion of each wafer was a rectangular chamber measuring 40 × 20 mm. Thin (0.1-mm) silastic sheets formed the sensing membrane. We determined the optimal chamber volume for pressure measurement by compressing the sensor within a sealed bell jar at different pressures up to 50 cm H_2O. The wafer's chamber volume was adjusted so that the wafer pressure accurately reflected the jar pressure (± 0.5 cm H_2O) throughout the range. Correct positioning of the wafers was confirmed in all animals at the time of computed tomographic (CT) scanning.

Flow rates, VT, Paw, Pes, and wafer pressures were simultaneously recorded on a chart recorder (9500; Astro-Med, West Warwick, RI) and stored on digital tape (RD-III T; TEAC, Tokyo, Japan).

Experimental Protocol

Respiratory failure was induced by injecting equal aliquots of oleic acid in supine and both lateral positions in a random sequence (total: 0.06 to 0.09 ml/kg). At the completion of oleic acid administration, mean ratio of arterial oxygen tension to fraction of inspired oxygen (Pa_{O_2}/FI_{O_2}) was 146.8 mm Hg (± 27.2 mm Hg), and mean arterial pressure was 90.8 mm Hg (± 17.0 mm Hg). After a 90-min equilibration period to stabilize injury, the dog was transferred from the laboratory to the CT scan facility. We employed a Siemens DRH (Forchheim, Germany) scanner, and exposures were taken at 120 kV, 50 mA, and 5 s. After obtaining a frontal tomogram of the chest, the CT scanner was positioned at the lung bases in position such as to avoid the appearance of the diaphragm dome even at the lowest pressure used (end-expiration at 5 cm H_2O positive end-expiratory pressure [PEEP]). This scanner position was maintained throughout the entire imaging phase of the experiment.

Each dog was studied at two levels of PEEP (5 and 15 cm H_2O) and three levels of VT (low = 11.9 ± 1.2 ml/kg, medium = 23.9 ± 2.5 ml/kg, and high = 35.8 ± 3.8 ml/kg) in random sequence. VT values were chosen so to apply sufficient pressure to achieve total lung capacity (TLC) and full lung recruitment, for defining its mechanisms. FI_{O_2} (80%) and respiratory rate were kept constant throughout the entire experimental protocol (13.2 ± 1.1 breaths/min). Each different PEEP–VT combination was applied for a minimum of 15 min before CT scanning. CT scans, limited to single slices acquired at both extremes of the tidal cycle, were taken under static conditions (end-inspiratory and end-expiratory pressure). A complete set of mechanical and gas exchange data was collected at the same time of CT scanning. All animals subjected to the protocol survived to its completion.

Image Analysis

We analyzed the CT images of the lung to which the wafers were applied, according to the method previously described (7). The outline of each lung was established by visual inspection of the CT section, drawing the outer boundary along the inside of the ribs and the inner boundary along the mediastinal organs. We then divided the total height of the CT section—i.e., the distance between the ventral and the dorsal surfaces of the CT section—into two levels (ventral, nondependent, and dorsal, dependent, halves of the lung).

Each CT section is comprised of voxels of dimension 0.15 × 0.15 × 0.9 cm. Each voxel is characterized by a CT number, expressed in Hounsfield units (HU), that ranges from +1,000 HU (bone), through 0 HU (water), to −1,000 HU (air). The frequency distribution of the CT numbers was computed as the frequency of voxels with CT numbers between −1,000 HU and −900 HU, between −900 HU and −800 HU, etc. until 0 HU and +100 HU.

Definitions

The following variables were measured or computed for each experimental condition:

1. *TLC of the whole lung (TLC_{WL}).* lung volume at end-inspiration and high VT (54 ± 4.3 cm H_2O plateau pressure) starting from 15 cm H_2O PEEP. TLC_{WL} was computed as 15 cm H_2O × compliance + inspired VT. The compliance arbitrarily used for this computation was the chord compliance measured between 15 cm H_2O of PEEP and the plateau pressure measured at low VT (averaged 27 ± 1.7 cm H_2O). The lung volumes measured in every other experimental condition were then expressed as a fraction of TLC_{WL}.
2. *Esophageal pressure (Pes).* the pressure recorded in the esophagus.
3. *Nondependent, middle, and dependent Ppl.* the pressures measured by wafers in the nondependent, middle, and dependent lung regions.
4. *Total vertical Ppl gradient.* the difference between the nondependent and dependent Ppl.
5. *Transpulmonary pressure (P_L).* the difference between Paw and Ppl measured by wafers.

CT-derived variables:

1. *CT gas volume.* the amount of gas measured in the CT section at any given experimental condition. It was computed as: gas volume = volume × CT/−1,000, where the volume is either the CT section area or the lung level area (in cm^2) multiplied by the cephalocaudal thickness (0.9 cm); CT is the mean CT number of the considered area, expressed in HU .
2. *TLC of the CT slice (TLC_{CT}).* arbitrarily defined as the gas volume measured in the CT slice at maximal inflation (54 ± 4.3 cm H_2O plateau pressure, starting from 15 cm H_2O of PEEP). The CT gas volumes measured in every other experimental condition were expressed as a fraction of TLC_{CT}.
3. *Nonaerated tissue.* the amount of gas-free tissue. This variable was computed first by establishing the frequency of voxels with CT number between −100 HU and +100 HU (7). This frequency was then multiplied by the volume of the CT section or the lung level volume. The voxels within −100 HU and 0 HU are not strictly "gas-free," as they have a gas-tissue ratio between 1⁄10 and zero. However, they were included in the "nonaerated tissue" compartment as they may represent the small airway collapse in which some gas is left in the pulmonary unit behind the collapsed bronchiolus (4).
4. *Hyperinflated tissue.* the fraction of CT numbers included within the range: (−1,000 HU to −900 HU), as suggested by Vieira and coworkers (8). This compartment represents a gas overfilling (−1,000 HU = all gas; −900 HU = gas-tissue ratio of 9/1). Note: hyperinflation refers to excessive gas content and not necessarily to overstretching, which relates to increased alveolar wall tension. A lung can be overstretched but not overfilled with air (and vice versa).
5. *Superimposed pressure.* a computation of hydrostatic pressure assuming that pressure is transmitted through the lung parenchyma as in a fluid (9), i.e., density times the height. Accordingly,

$$P = (1 - CT/-1{,}000) \times \text{height}.$$

   Therefore, the superimposed pressure in the ventral, nondependent half of the lung was computed as the product of the average CT number of the upper half lung times one-half of the total height of the CT section. The superimposed pressure of the dorsal, dependent half of the lung was computed as the average CT number of this lower half of the lung times one-half of the total height of the CT section. The total superimposed pressure was computed as the sum of the superimposed pressure of the nondependent lung and the superimposed pressure of the dependent lung.
6. *Transalveolar pressure.* in each CT slice, the difference between the superimposed pressure and Paw at a given lung level, according to Hickling (10). Thus, a positive value indicated that the compressive pressure is higher than the applied Paw in a given lung region.
7. *Potential for recruitment and fractional recruitment.* The potential for recruitment was defined as the difference between the maximal amount of nonaerated tissue (measured at 5 cm H_2O PEEP and low VT) and the minimal amount of nonaerated tissue (measured at 54 ± 4.3 cm H_2O plateau pressure and 15 cm H_2O of PEEP). The fractional recruitment for the entire CT slice was expressed as:

   1 − (observed inspiratory nonaerated tissue − least amount of nonaerated tissue/potential for recruitment).

8. *Volume and recruitment pressure curves.* These curves were constructed by plotting the inspiratory plateau pressure (*x*-axis) versus the percentage of the TLC_{WL} and the TLC_{CT} (VP curve of the whole lung and VP curve of the lung CT slice, respectively—*y*-axis) or versus the fractional recruitment (recruitment pressure curve—*y*-axis). The data for VP curve and recruitment pressure curve were fitted with the sigmoid function $y = a / \{1 + \exp [-(x - x_0) / b]\}$, where a corresponds to the vital capacity, b is a parameter propor-

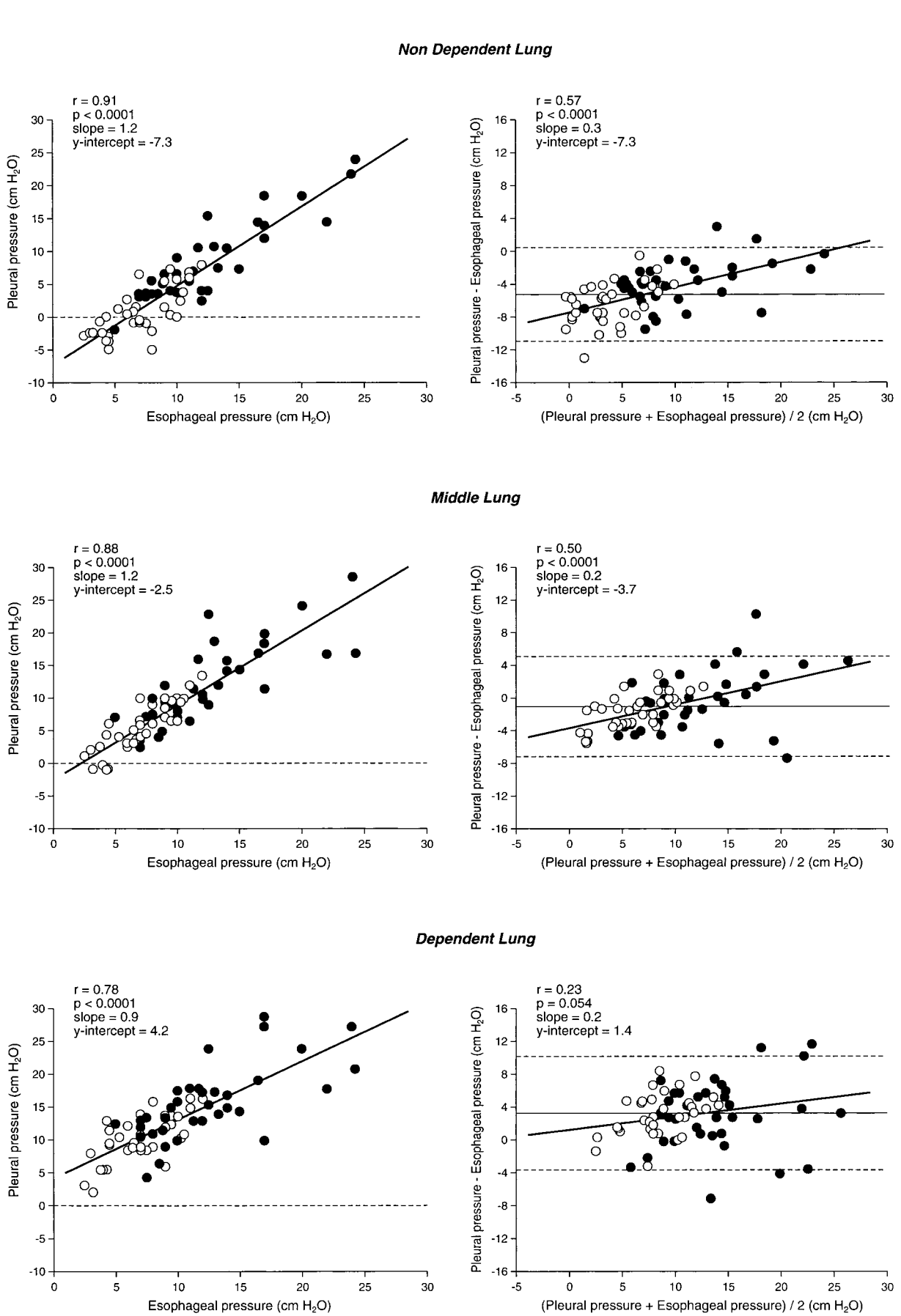

Figure 1. Relationship between Pes and Ppl in the nondependent (*upper panel*, left), middle (*middle panel*, left) and dependent lung (*lower panel*, left). The corresponding Bland and Altman analyses are shown on the right side of the figure. Each experimental point has been plotted (6 end-inspiratory points per dog, *closed circles*; 6 end-expiratory points per dog, *open circles*—72 total data points). The linear regression parameters are displayed in each panel. In the right panels, *solid line* and *dashed lines* represent the mean ± 2 SD of the difference between Ppl and Pes.

tional to the pressure range within which most of the volume change takes place, and x_0 is the pressure at the inflection point of the sigmoidal curve (where curvature changes sign), according to Venegas and coworkers (11).

9. *Estimated threshold opening pressure (TOP).* the Paw at which new increment of recruitment was observed during inflation. The data points were derived from the fitted recruitment pressure curve obtained in each animal. Interpolation was done to obtain the estimated TOP at 5 cm H_2O pressure intervals. Thus, data are not strictly experimental but an estimate of the TOP. Frequency distributions of estimated TOPs were fitted with a gaussian function ($y = a * \exp\{-0.5\,[(x - x_0) / b]^2\}$).

Statistical Analysis

All data are expressed as mean ± SEM. Regression analysis was performed with the least-squares method. Pes and Ppl were compared using regression analysis and Bland and Altman analysis (12). Values obtained at different levels of PEEP and inspiratory plateau pressure were compared using a two-way analysis of variance (ANOVA) for repeated measures. Individual comparisons were performed using the paired *t* test; Bonferroni's correction was applied for multiple comparisons. Statistical significance was accepted as $p < 0.05$.

RESULTS

Pleural Pressure and Esophageal Pressure

In Figure 1 we report the relationship between Ppl and Pes in the nondependent, middle, and dependent lung regions, as well as the Bland and Altman analysis of each relationship. As shown, there is a good correlation between the Pes and Ppl. The absolute value of Pes, however, only serves as a good estimate of Ppl for the middle lung regions, being consistently different from the Ppl measured by the wafer values in the nondependent and in the dependent lung regions. Moreover, the Bland and Altman analysis reveals that Pes slightly but systematically underestimates the Ppl when Paw increases.

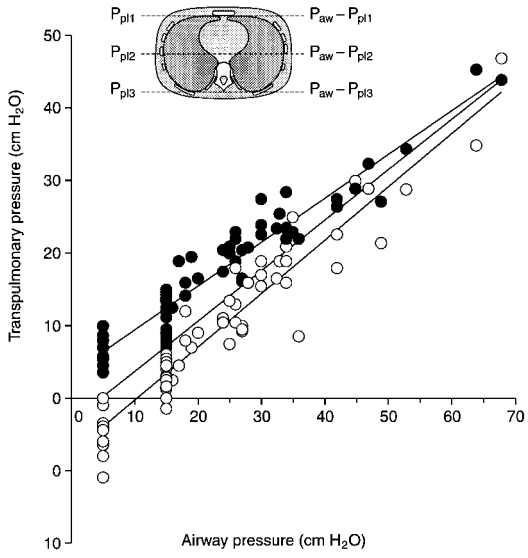

Figure 2. Paw and P_L relationship. *Solid circles* and *upper regression line* refer to the nondependent lung regions ($P_L = 3.3 + 0.6 \times Paw$, $r = 0.96$, $p < 0.0001$); *open circles* and *lower regression line* refer to the dependent lung regions ($P_L = -7.7 + 0.7 \times Paw$, $r = 0.96$, $p < 0.0001$). The *middle regression line* depicts the relationship for the middle lung regions (single points are not shown for clarity) ($P_L = -3.2 + 0.7 \times Paw$, $r = 0.93$, $p < 0.0001$). Seventy-two data points are displayed for each regression relationship and the points refer both to end-inspiration and end-expiration. The schema refers to the lung regions in which the Ppl measurements were taken. Ppl_1 is the Ppl measured by the wafer in the nondependent lung region; Ppl_2 is the Ppl measured by the wafer in the middle lung region; Ppl_3 is the Ppl measured by the wafer in the dependent lung region. Accordingly, the corresponding P_L were $Paw - Ppl_1$, $Paw - Ppl_2$, and $Paw - Ppl_3$.

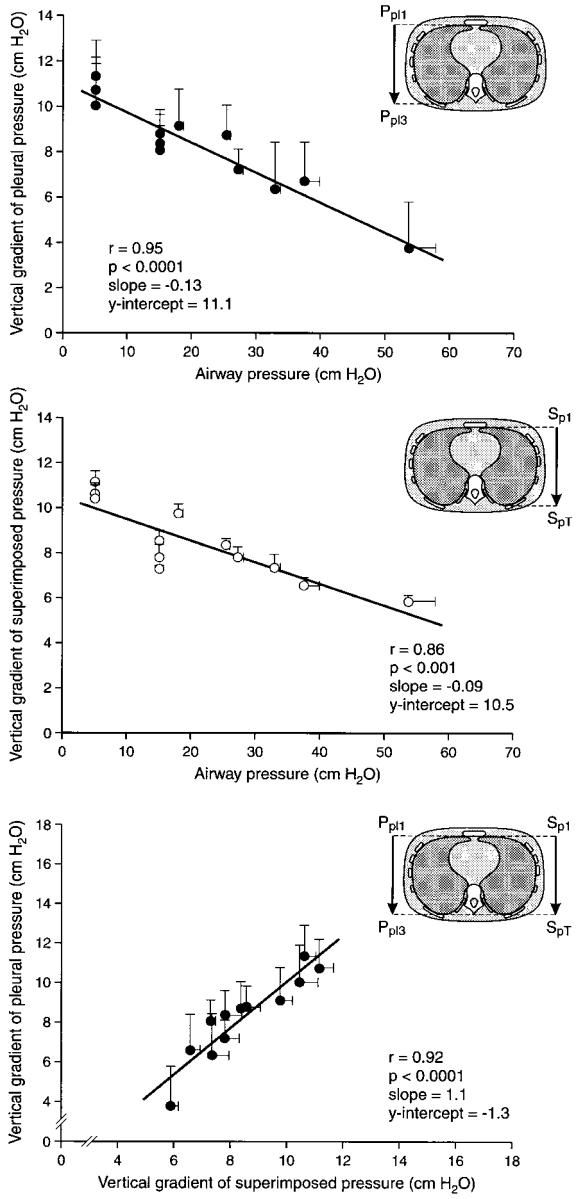

Figure 3. *Upper panel*: Vertical gradient of Ppl as a function of the Paw. Each point represents the average of these two variables obtained in the six dogs at each experimental step (6 at end-expiration and 6 at end-inspiration). *Middle panel*: Vertical gradient of superimposed pressure as a function of Paw. As in the *upper panel*, each point represents the average of these two variables obtained in the six dogs for each experimental step (6 at end-expiration and 6 at end-inspiration). *Lower panel*: Vertical gradient of Ppl, directly measured by the wafers, as a function of the vertical gradient of superimposed pressure. Each point represents the average of these two variables obtained in the six dogs for each experimental step (6 at end-expiration and 6 at end-inspiration). For clarity, the CT schema in each panel represents the variable analyzed. Ppl_1 is the Ppl measured by the wafer in the nondependent lung region; Ppl_3 is the Ppl measured by the wafer in the dependent lung region; Sp_1 is the superimposed pressure in the nondependent lung region (zero cm H_2O); Sp_T is the total superimposed pressure present at the dependent lung region. The vertical gradient of pleural pressure ($Ppl_3 - Ppl_1$) equals in absolute number the vertical gradient of P_L (P_L1–P_L3). The linear regression parameters are displayed in each panel. Data are expressed as mean ± SEM.

TABLE 1. POTENTIAL FOR RECRUITMENT*

	Potential for Recruitment (*g*)	Total Parenchyma Tissue (*g*)	Potential for Recruitment (%)
Dog 1	41.5	58.4	71.1
Dog 2	26.9	68.8	39.1
Dog 3	42.4	83.4	50.9
Dog 4	31.2	62.1	50.2
Dog 5	35.9	71.8	50.0
Dog 6	34.5	67.8	50.8
Mean	35.4	68.7	52.0
SD	6.0	8.7	10.4
SEM	2.4	3.5	4.2

* The percentage of potential for recruitment was computed as potential for recruitment, expressed in grams, normalized for total lung tissue included in the slice, expressed in grams.

Vertical Gradient of Ppl and Superimposed Pressure

In Figure 2, we report the P_L measured in the nondependent, middle, and dependent lung regions as a function of the pressure applied to the airway (both at end-expiration and at end-inspiration). In this set of animals, P_L was negative at end-expiration with PEEP 5 cm H_2O in the dependent regions, implying lung collapse.

The relationship between the vertical gradient of P_L (which equals the vertical gradient of Ppl) and the applied Paw is reported in Figure 3, *upper panel*. As shown, the vertical gradient almost halved as Paw increased from 5 to 54 cm H_2O. The superimposed pressure, when increasing the applied Paw, behaved similarly (Figure 3, *middle panel*). This suggests that the vertical gradient of Ppl is mostly explained by gravitational forces, as shown in Figure 3, *lower panel*, which illustrates the relationship between the vertical gradient of Ppl and the superimposed pressure ($r = 0.92$, $p < 0.0001$, slope = 1.1, *y*-intercept = -1.3 cm H_2O).

Potential for Recruitment

As shown in Table 1, oleic acid injury is associated with a huge potential for recruitment. In fact, at 5 cm H_2O PEEP and low V_T, approximately 50% of the lung tissue is nonaerated, whereas at the maximal pressure used (54 ± 4.3 cm H_2O), only 4% of the lung parenchyma is nonaerated. This suggests that, in this model, the loss of aeration is primarily due to collapse.

Inflation and Recruitment

The behavior of the VP curve of the lung CT slice closely reflects the behavior of the VP curve of the whole lung, as shown in Figure 4. In fact, the regression between the TLC_{CT} gas fraction and the TLC_{WL} gas fraction approaches the identity (not shown, $r = 0.97$, $p < 0.0001$, slope = 0.90 and *y*-intercept = 0.04%). As shown in Figure 4, both relationships present the classic sigmoid shape, with both lower and upper inflection points ($r = 0.96$, $p < 0.0001$, and $r = 0.97$, $p < 0.0001$ for the VP curve of the lung CT slice and whole lung, respectively).

Expressing recruitment as a fraction of the potential for recruitment available (Figure 5, *upper panel*), it appears that recruitment presents a sigmoid shape ($r = 0.95$, $p < 0.0001$), proceeding continuously along the VP curve, across the upper and lower inflection regions. In fact, the increase of percent of recruitment equals the increase of percent of inflation, and the

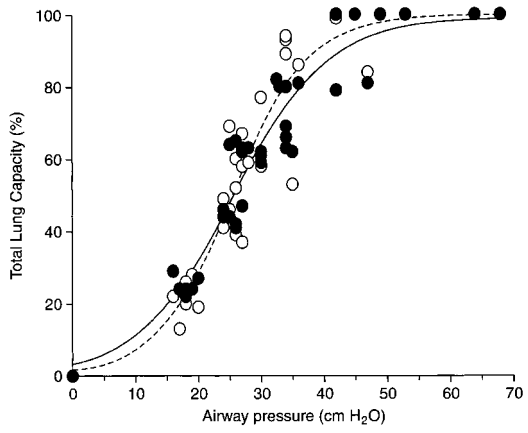

Figure 4. VP curve for the whole lung and for the lung CT slice. Volume is expressed as a percentage of TLC. *Solid circles* and *solid line* refer to the whole lung ($r = 0.97$, $p < 0.0001$); *open circles* and *dashed line* refer to the lung CT slice ($r = 0.96$, $p < 0.0001$). Each data point refers to the single experimental point obtained at end-inspiration (6 points per dog, 36 total points for the whole lung, and 36 total points for the lung CT slice). The data indicate that the single CT slice reasonably represents whole lung behavior.

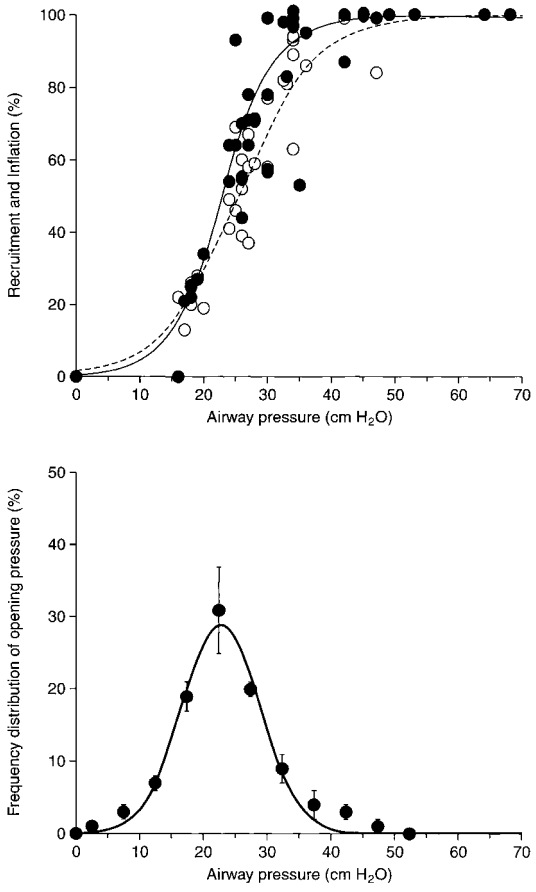

Figure 5. *Upper panel*: recruitment as a function of Paw. *Solid circles* and *solid line* refer to fractional recruitment ($r = 0.95$, $p < 0.0001$); *open circles* and *dashed line* refer to the fractional inflation of the lung CT slice ($r = 0.96$, $p < 0.0001$). Each point refers to a single experimental condition at end-inspiration (6 points per dog, 36 total points for recruitment pressure curve, and 36 total points for VP curve). *Lower panel*: frequency distribution of estimated threshold opening pressures as a function of Paw ($r = 0.99$, $p < 0.0001$). Each point has been computed at each 5 cm H_2O pressure interval from the fitted recruitment pressure curve obtained in each dog. Thus, these points are not experimental but estimates of the threshold opening pressures. Data are expressed as mean ± SEM.

TABLE 2. END-INSPIRATORY AND END-EXPIRATORY COLLAPSE*

		5 cm H_2O PEEP			15 cm H_2O PEEP		
	Tidal Volume (*ml/kg*)	Low V_T 11.9 ± 0.5	Medium V_T 23.9 ± 1.0	High V_T 35.8 ± 1.6	Low V_T 11.9 ± 0.5	Medium V_T 23.9 ± 1.0	High V_T 35.8 ± 1.6
Inspiration	Plateau, cm H_2O	18.0†‡ ± 0.6	25.3†‡ ± 0.5	32.8†‡ ± 0.9	27.2‡ ± 0.7	37.4‡ ± 2.4	53.5‡ ± 4.3
	P_L1, cm H_2O	16.3 ± 1.1	20.3† ± 0.8	25.0†§ ± 1.0	19.7‡ ± 1.1	25.3‡ ± 1.6	34.6‡ ± 3.4
	P_L2, cm H_2O	11.7 ± 1.1	16.1 ± 1.2	20.2†§ ± 1.6	14.7‖ ± 1.8	21.1‖ ± 2.2	33.4 ± 5.9
	P_L3, cm H_2O	7.2‖ ± 1.4	11.6‖ ± 1.5	18.7† ± 1.4	12.5‡ ± 1.2	18.7‡ ± 2.7	30.9‡ ± 3.8
	Nonaerated tissue tot, g	30.2†‡ ± 1.9	17.5†‡ ± 2.2	10.2†‡ ± 3.6	10.5 ± 2.5	5.2 ± 1.0	2.8§ ± 0.4
	Upper (nondependent), g	1.1¶ ± 0.2	1.1¶ ± 0.4	1.1¶ ± 0.2	1.2¶ ± 0.4	1.2 ± 0.3	1.1 ± 0.3
	Lower (dependent), g	29.2†‡ ± 1.8	16.4†‡ ± 2.1	9.1†‡ ± 3.6	9.3 ± 2.2	4.0§ ± 1.0	1.7§ ± 0.4
Expiration	PEEP, cm H_2O	5† ± 0.0	5† ± 0.0	5† ± 0.0	15 ± 0.0	15 ± 0.0	15 ± 0.0
	P_L1, cm H_2O	7.1† ± 0.8	6.4† ± 0.5	6.4† ± 1.1	11.9 ± 1.1	11.0 ± 1.1	9.8§ ± 1.0
	P_L2, cm H_2O	1.3† ± 1.0	0.4† ± 1.4	0.3† ± 1.3	6.8 ± 1.3	6.1 ± 1.2	5.8 ± 1.6
	P_L3, cm H_2O	−3.6† ± 0.9	−4.9† ± 1.4	−3.7† ± 1.1	3.1 ± 1.0	2.6 ± 1.0	1.8 ± 0.8
	Nonaerated tissue tot, g	38.1† ± 2.5	29.1†§ ± 2.6	24.8†§ ± 4.4	12.1 ± 2.6	8.3 ± 2.4	4.9§ ± 0.7
	Upper (nondependent), g	2.3¶ ± 0.5	2.1¶ ± 0.6	3.0¶ ± 1.1	1.5¶ ± 0.4	1.0¶ ± 0.3	1.4 ± 0.2
	Lower (dependent), g	35.9† ± 2.2	27.1†§ ± 2.7	21.8†§ ± 4.5	10.5 ± 2.4	7.3 ± 2.2	3.5§ ± 0.7

Definition of abbreviations: Lower (dependent) = nonaerated tissue of the lower half of the lung CT slice; Nonaerated tissue tot = nonaerated tissue of the whole lung CT slice; P_L1 = transpulmonary pressure in the nondependent lung regions; P_L2 = transpulmonary pressure in the middle lung regions; P_L3 = transpulmonary pressure in the dependent lung regions; Plateau = inspiratory plateau pressure; Upper (nondependent) = nonaerated tissue of the upper half of the lung CT slice.

* Data are expressed as mean ± SEM.

† $p < 0.05$ compared with 15 cm H_2O at the same V_T.

‡ $p < 0.05$ compared with other V_T at the same PEEP level.

§ $p < 0.05$ compared with low V_T at the same PEEP level.

‖ $p < 0.05$ compared with high V_T at the same PEEP level.

¶ $p < 0.05$ compared with lower region at the same PEEP level and V_T.

regression (not shown) is close to identity ($r = 0.94$, $p < 0.0001$, slope = 1.01 and *y*-intercept = 0.06%). From the same data, it is possible to compute the frequency distribution of the estimated TOP, which fits a gaussian function ($r = 0.99$, $p < 0.0001$); this analysis is reported in Figure 5 (*lower panel*). As shown, the maximal frequency of estimated TOPs occur at a pressure between 20 and 25 cm H_2O.

The topology of recruitment appears to follow a definite spatial pattern. Table 2 summarizes the most relevant mechanical and CT findings. In the upper lung the recruitment is negligible, whereas most recruitment is observed in the lower (dependent) regions of the slice. Interestingly, even at the highest pressures (54 ± 4.3 cm H_2O) we did not find any sign of hyperinflation, as defined by an increased frequency of CT numbers in the relevant compartment −1,000 HU to −900 HU. In fact, this "hyperinflation compartment" never exceeded 4% of the entire CT frequency distribution throughout the experiment. This suggests that hyperinflation (i.e., gas overfilling) and overstretching (i.e., increased alveolar wall tension) may be two independent phenomena, as overstretching causes the VP curve to flatten at the highest pressure, without evidence for hyperinflation.

End-expiration

The most striking finding at end-expiration was that, at the same end-expiratory Paw and P_L, the amount of nonaerated tissue significantly differed, depending on whether ventilation was performed at low, medium, or high V_T. A representative CT scan illustrating this phenomenon is shown in Figure 6. The details of the CT variables as well as the corresponding P_L are reported in Table 2.

Interactions between End-expiratory and End-inspiratory Pressures

The interactions between end-inspiratory and end-expiratory phenomena are summarized in Table 2 and in Figure 7, in which the end-expiratory nonaerated tissue appears to be a

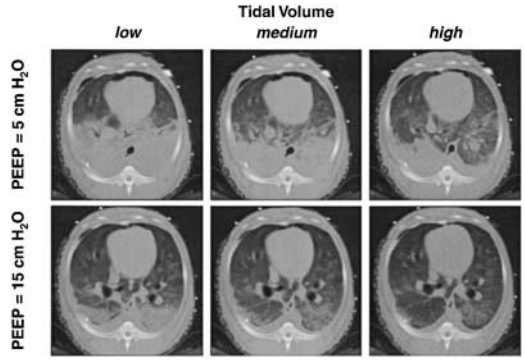

Figure 6. A representative CT scan obtained in one dog at end-expiration for each experimental step. At a similar PEEP level, either 5 or 15 cm H_2O, the amount of end-expiratory collapse was dramatically different, depending on whether ventilation was performed at low, medium, or high V_T.

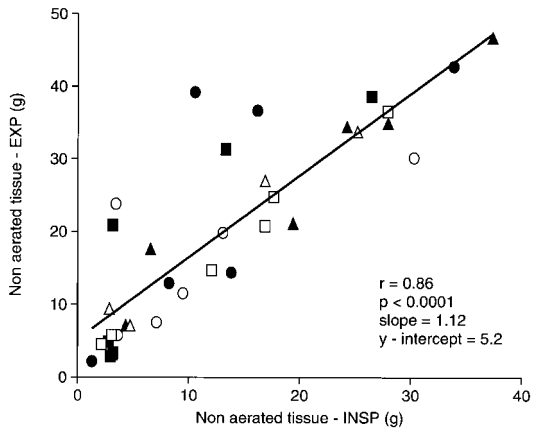

Figure 7. End-expiratory nonaerated tissue as a function of end-inspiratory nonaerated tissue. *Solid circles* refer to Dog 1; *open circles*, Dog 2; *solid triangles*, Dog 3; *open triangles*, Dog 4; *solid squares*, Dog 5; *open squares*, Dog 6.

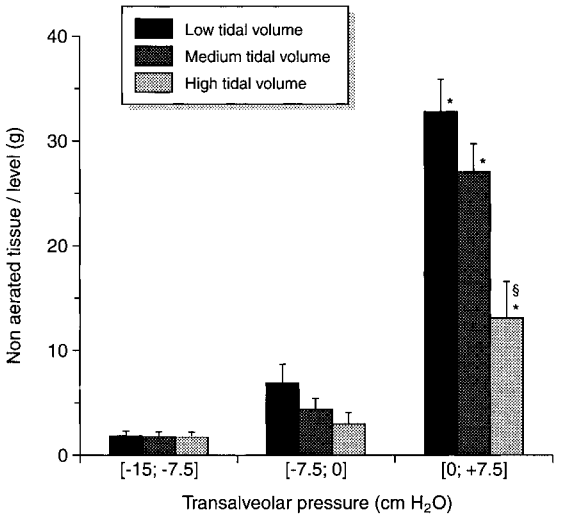

Figure 8. Nonaerated tissue, at end-expiration, either in the lower or the upper lung level as a function of the transalveolar pressure measured at that level. Data are expressed as mean ± SEM. *$p < 0.001$ compared with other transalveolar pressures at the same V_T and minute ventilation ($\dot{V}_E$). §$p < 0.001$ compared with other V_T and $\dot{V}_E$ at the same transalveolar pressure.

function of end-inspiratory nonaerated tissue ($r = 0.86$, $p < 0.0001$, slope = 1.12 and *y*-intercept = 5.2 g). This suggests that as more tissue is recruited at the end of inspiration, more remains recruited at the end of expiration (i.e., the less the inspiratory collapse, the less end-expiratory collapse), despite identical PEEP and end-expiratory P_L. However, whatever the extent of opening may be at the end of inspiration, the superimposed pressure seems to play a crucial role in encouraging end-expiratory collapse. If the superimposed pressure in a given lung region is higher than the applied Paw (i.e., the transalveolar pressure is positive), collapse will occur. This phenomenon is shown in Figure 8.

Gas Exchange

The arterial blood gases and pH measured under different experimental conditions are reported in Table 3. Whereas the Pa_{CO_2} and pH changed significantly with V_T but not with PEEP, the oxygenation improved with increases in either V_T or PEEP. Oxygenation closely paralleled changes in the amount of nonaerated tissue, both in inspiration and in expiration. We observed a significant correlation between these two variables: $\Delta\ Pa_{O_2} = -32.3$ mm Hg $-8.9 \times \Delta$ inspiratory nonaerated tissue ($r = 0.75$, $p < 0.0001$); $\Delta\ Pa_{O_2} = -11.9$ mm Hg $-7.3 \times \Delta$ expiratory nonaerated tissue ($r = 0.80$, $p < 0.0001$).

DISCUSSION

Pleural, Esophageal, and Superimposed Pressure

In this experimental study, we aimed first to define the relationship between Pes and the lung surface pressures actually measured at three vertical levels in the supine chest. As previous work (9) had strongly suggested that the gravitational forces may play a substantial role in the distribution of lung collapse, we chose to measure the Ppl of these supine animals along the vertical axis in nondependent, middle, and dependent regions. Using computed tomography, we could also estimate superimposed pressure as the product of density × the vertical height, i.e., assuming that the hydrostatic forces are transmitted through the lung parenchyma as in a fluidlike sponge model (13, 14). Thus, we aimed to answer two questions: (*1*) To what degree does the Pes estimate pleural surface pressures in a partially collapsed lung? (*2*) What is the role of the superimposed pressure in determining the vertical gradients of Ppl and P_L along the vertical axis?

The relationship between the Pes and the pleural surface pressures measured directly in nondependent, middle, and dependent lung regions at different Paw under static conditions (no flow) is illustrated in Figure 1. Pes more closely reflected midlung surface pressure in these supine animals. A close correspondence between Pes and lateral lung surface pressure has also been previously demonstrated in the normal uninjured dog (15). Despite the significant differences we found between the absolute values of Pes and the pressures measured at various sites along the pleural surface, the changes of all measures of Ppl were similar in response to increasing Paw, suggesting that the variation of Pes (which is the most clinically relevant measurement) is a reasonable estimate of the variations of Ppl, as previously suggested (16). When measuring Pes, however, it is worth considering that the absolute pleural surface pressures in this model are approximately 7 cm H_2O lower than Pes in the nondependent regions and 4 cm H_2O higher in the dependent regions at low intrathoracic pressure. With increasing pressures, however, there is a progressive underestimate of true Ppl by Pes. This phenomenon is present, in varying degrees, in nondependent, middle, and dependent lung regions (*see* Bland and Altman analysis, Figure 1).

The vertical gradient of Ppl is of clinical relevance, as it determines the regional P_L, the distending force of the lung. Before inducing respiratory failure in these six dogs, we measured a vertical gradient between nondependent and dependent Ppl at end-expiration of 6.8 ± 0.9 cm H_2O. The end-expiratory gradient of lung surface pressure increased significantly after the induction of respiratory failure (vertical gradient = 11.3 ± 1.6 cm H_2O, $p < 0.05$). Interestingly, as previously observed in normal humans and animals (17, 18), the vertical gradient of

TABLE 3. GAS EXCHANGE*

	5 cm H_2O PEEP			15 cm H_2O PEEP		
Tidal Volume (*ml/kg*)	Low V_T 11.9 ± 0.5	Medium V_T 23.9 ± 1.0	High V_T 35.8 ± 1.6	Low V_T 11.9 ± 0.5	Medium V_T 23.9 ± 1.0	High V_T 35.8 ± 1.6
Pa_{O_2}, mm Hg	76.2†‡ ± 7.8	97.3†‡ ± 10.5	171.2† ± 38.1	186.3 ± 27.3	299.3§ ± 17.8	365.5§ ± 18.4
Pa_{CO_2}, mm Hg	83.3‖ ± 6.5	51.1†‖ ± 4.9	33.2‖ ± 2.2	84.8 ± 7.6	45.0§ ± 2.7	34.1§ ± 3.0
pH	6.99‖ ± 0.04	7.17‖ ± 0.04	7.31‖ ± 0.03	7.02 ± 0.09	7.19§ ± 0.04	7.29§ ± 0.05

Definition of abbreviations: RR = respiratory rate; $\dot{V}E$ = minute ventilation.
* Data are expressed as mean ± SEM.
† $p < 0.05$ compared with 15 cm H_2O at the same V_T.
‡ $p < 0.05$ compared with high V_T at the same PEEP level.
§ $p < 0.01$ compared with low V_T at the same PEEP level.
‖ $p < 0.05$ compared with other V_T at the same PEEP level.

pleural surface pressure tended to decrease as Paw increased. Several hypotheses have been advanced to explain this phenomenon. For example, as the nondependent regions near TLC, relatively less expansion occurs in those areas, limiting further increments in adjacent Ppl.

We also found a decrease of the superimposed pressure as Paw increased (i.e., at 5 cm H_2O PEEP and 54 ± 4.3 cm H_2O plateau pressure, the corresponding superimposed pressures were 10.7 ± 0.3 and 5.8 ± 2.8 cm H_2O, respectively, $p < 0.001$). One possible explanation for this decrease in superimposed pressure is systematic sampling error: as Paw increases, the CT slice "moves" with lung inflation. Thus, the lung units comprising the new lung CT slice after inflation may differ from those comprising the initial one. However, the decrease of superimposed pressure could also be a true phenomenon; it is possible that part of the "tissue" mass decreases because blood shifts out of the thorax as Paw and Ppl increase. Other explanations are also possible. If tissue density decreases more than lung height increases in response to elevating Paw, the superimposed pressure decreases, in a fluidlike model. Alternatively, if the lung is not considered as a fluid, if it retains the same mass and the dependent surface area increases with inflation, then the pressure (mass per unit area) decreases. Whatever the true explanation for the decrease of the superimposed pressure with lung inflation may be, we found a straightforward correspondence between the vertical gradient of Ppl and calculated superimposed pressure (Figure 3, *lower panel*). These data suggest that the superimposed pressure—with all the limitations of the basic assumption of a fluidlike model—is likely to be a major contributing factor to the vertical gradients of Ppl and P_L, which determine the tendency for regional lung collapse.

Thus, we may conclude that: (*1*) Pes is a reasonable estimate of Ppl in the zone between the nondependent and dependent lung regions, (*2*) its variations approximate the variations of the lung surface pressures in all regions, (*3*) there is a slight systematic underestimation of pleural surface pressure by Pes when increasing Paw, and (*4*) the superimposed pressure is likely to be an important (if not the primary) determinant of the vertical Ppl gradient in this setting.

Inflation and Recruitment

In this experimental setting, the single CT slice appears a reasonable estimate of the behaviors of the whole lung (*see* Figure 4), as previously observed (19). If so, approximately 50% of the lung appears nonaerated at 5 cm H_2O PEEP. Because only 4% of the lung parenchyma remained nonaerated at 54 ± 4.3 cm H_2O inspiratory pressure, the underlying pathology of the oleic acid model seems to be one of primarily lung collapse. Indeed, this model is characterized by a huge potential for recruitment, and proves to be perfectly suitable to study the recruitment and derecruitment mechanism.

Perhaps the most important finding of our study is that recruitment proceeds along the entire inspiratory limb of the VP curve (as shown in Figure 5). It is important to point out, however, that VP curve was not constructed through a continuous process (as with supersyringe or low-flow technique); rather, single points on the curve were recorded at least 15 min apart. Moreover, Paw were not increased as a function of time, as during the classic VP curve, but were applied randomly. Thus, we cannot say that the VP curve we constructed in this setting is equivalent to the VP curve obtained by the method used in clinical practice. It is worth noting however, that when we constructed VP curves in human patients with the method used here (discontinuous) and with the standard supersyringe method (continuous), we found them to be virtually superimposed (20).

The observation that recruitment occurs continuously along the entire VP curve may have several clinical implications: first, the VP curve may be seen as equivalent to a recruitment pressure curve, as previously suggested on theoretical grounds (21); second, setting the PEEP (which is an expiratory maneuver) according to the inspiratory lower inflection point does not seem to have a good pathophysiologic rationale. At this level of pressure, only about 20% of the recruitment had been accomplished in these dogs. Unfortunately, the recruitment pressure curve does not tell the absolute amount of recruitment, but only the fraction of the potential for recruitment which has been exploited at a given pressure. It is also of interest to consider the frequency distribution of the estimated TOP (*see* Figure 5). Under our experimental condition, the estimated TOPs cover a wide range (from 10 cm H_2O end to 50 cm H_2O), with the greatest frequency of opening occurring at around 25 cm H_2O. Pressures of the latter magnitude are reported to be required to reverse small airway collapse (22), whereas higher pressures are required to open lung units when collapse originates at the alveolar level. If so, in the oleic acid model, it seems that the collapse is primarily (but not only) due to small airway closure.

End-expiratory Collapse and Its Interactions with Inspiratory Pressures

At the same levels of end-expiratory and transpulmonary pressures (whether assessed in the nondependent, middle, or dependent lung regions), the extent of end-expiratory collapse (i.e., the amount of nonaerated tissue) depended on the previous V_T (and pressures) in use (Figure 7 and Table 2). The most likely explanation for this volume history dependence is that at smaller V_T lung parenchyma stayed collapsed at end-expiration simply because it had not been exposed to sufficient Paw to open during the previous inspiration. This finding stresses the concept that the process of recruitment is an inspiratory phenomenon, which profoundly affects the extent of end-expiratory collapse (*see* Figure 8).

The extent of end-expiratory collapse, however, is not only a function of the preceding inspiratory pressure achieved by the V_T ("opening" pressure), but also of the pressure at the end of expiration acting to keep open units patent. As an example, at a high V_T and 5 cm H_2O PEEP the average amount of end-inspiratory collapsed tissue was 10.2 ± 3.6 g (33 ± 0.9 cm H_2O plateau) (Table 2). The same amount of end-inspiratory collapsed tissue (10.5 ± 2.5 g) was observed at low V_T (27 ± 0.7 cm H_2O plateau) and 15 cm H_2O PEEP. This indicates that in that range of inspiratory pressure (27 to 33 cm H_2O) the end-inspiratory "opening" was substantially the same. However, at the end of expiration, the amount of the collapse was greater at 5 cm H_2O of PEEP (24.8 ± 4.4 g) compared with 15 cm H_2O (12.1 ± 2.6 g, $p < 0.01$). The reason may be shown in Figure 8. Transalveolar pressure was positive at 5 cm H_2O, i.e., the superimposed pressure was higher than PEEP, encouraging collapse. On the contrary, at 15 cm H_2O PEEP the transalveolar pressure was negative, i.e., the superimposed pressure was lower than PEEP and what was open during the inspiration stayed open at the end of expiration.

However, it is also possible that the level of end-expiratory collapse influences the end-inspiratory collapse. As shown in Table 2, at similar level of end-inspiratory pressure (25.3 ± 0.1 cm H_2O versus 27.2 ± 0.7 cm H_2O, medium V_T at 5 cm H_2O PEEP and low V_T at 15 cm H_2O PEEP) the end-inspiratory collapse was 17.5 ± 2.2 g versus 10.5 ± 2.5 g ($p < 0.01$). To exactly define which is the independent variable (end-inspiration or end-expiration) a different experimental design is

required. These findings, however, stress the concept that end-inspiratory and end-expiratory collapse are interdependent.

In this experimental model with a high potential for recruitment, we found a strong dependency of end-expiratory collapse on both inspiratory and superimposed pressures. It remains to demonstrate the applicability of these "rules" to the human with ALI/ARDS.

References

1. International consensus conferences in intensive care medicine. Ventilator-associated lung injury in ARDS American Thoracic Society, European Society of Intensive Care Medicine, Societe de Reanimation Langue Francaise. *Intensive Care Med* 1999;25:1444–1452.
2. The Acute Respiratory Distress Syndrome Network. Ventilation with lower tidal volumes as compared with traditional tidal volumes for acute lung injury and the acute respiratory distress syndrome. *N Engl J Med* 2000;342:1301–1308.
3. Muscedere JG, Mullen JBM, Gan K, Slutsky AS. Tidal ventilation at low airway pressures can augment lung injury. *Am J Respir Crit Care Med* 1994;149:1327–1334.
4. Gattinoni L, Pelosi P, Crotti S, Valenza F. Effects of positive end-expiratory pressure on regional distribution of tidal volume and recruitment in adult respiratory distress syndrome. *Am J Respir Crit Care Med* 1995;151:1807–1814.
5. Lachmann B. Open up the lung and keep the lung open. *Intensive Care Med* 1992;18:319–321.
6. Baydur A, Bherakis PK, Zin WA, Jaeger M, Milic-Emili J. A simple method for assessing the validity of the esophageal balloon technique. *Am Rev Respir Dis* 1982;126:788–791.
7. Gattinoni L, Pesenti A, Avalli L, Rossi F, Bombino M. Pressure–volume curve of total respiratory system in acute respiratory failure. *Am Rev Respir Dis* 1987;136:730–736.
8. Vieira SRR, Puybasset L, Richecoeur J, Lu Q, Cluzel P, Gusman PB, Coriat P, Rouby JJ. A lung computed tomographic assessment of positive end-expiratory pressure-induced lung overdistention. *Am J Respir Crit Care Med* 1998;158:1571–1577.
9. Pelosi P, D'Andrea L, Vitali G, Pesenti A, Gattinoni L. Vertical gradient of regional lung inflation in adult respiratory distress syndrome. *Am J Respir Crit Care Med* 1994;149:8–13.
10. Hickling KG. The Pressure–Volume curve is greatly modified by recruitment: a mathematical model of ARDS lungs. *Am J Respir Crit Care Med* 1998;158:194–202.
11. Venegas JG, Harris RS, Simon BA. A comprehensive equation for the pulmonary pressure–volume curve. *J Appl Physiol* 1998;84:389–395.
12. Bland JM, Altman DG. Statistical methods for assessing agreement between two methods of clinical measurement. *Lancet* 1986;1:307–310.
13. Gattinoni L, D'Andrea L, Pelosi P, Vitale G, Pesenti A, Fumagalli R. Regional effects and mechanism of positive end-expiratory pressure in early adult respiratory distress syndrome. *JAMA* 1993;269:2122–2127.
14. Bone RC. The ARDS lung: new insights from computed tomography. *JAMA* 1993;269:2134–2135.
15. Gillespie DJ, Lai YL, Hyatt RE. Comparison of esophageal and pleural pressures in the anesthetized dog. *J Appl Physiol* 1973;35:709–713.
16. Cherniack RM, Fahri LE, Armstrong BW, Proctor DF. A comparison of esophageal and intrapleural pressure in man. *J Appl Physiol* 1955;8:203–211.
17. Agostoni E, D'Angelo E, Bonanni MV. Topography of pleural surface pressure above resting volume in relaxed animals. *J Appl Physiol* 1970;29:297–306.
18. Agostoni E, Miserocchi G. Vertical gradient of transpulmonary pressure with active and artificial lung expansion. *J Appl Physiol* 1970;29:705–712.
19. Gattinoni L, Pelosi P, Vitale G, Pesenti A, D'Andrea L, Mascheroni D. Body position changes redistribute lung computed tomographic densities in patients with acute respiratory failure. *Anesthesiology* 1991;74:15–23.
20. Crotti S, Mascheroni D, Caironi P, Pelosi P, Ronzoni G, Mondino M, Marini JJ, Gattinoni L. Recruitment and derecruitment during acute respiratory failure—a clinical study. *Am J Respir Crit Care Med* 2001;164:131–140.
21. Harris RS, Hess DR, Venegas JG. An objective analysis of the Pressure–Volume curve in the acute respiratory distress syndrome. *Am J Respir Crit Care Med* 2000;161:432–439.
22. Glaister DH, Schroter RC, Sudlow MF, Milic-Emili J. Transpulmonary pressure gradient and ventilation distribution in excised lungs. *Respir Physiol* 1973;17:365–385.